THE JOURNAL OF PHYSICAL CHEMISTRY Letters

pubs.acs.org/JPCL Letter

Role of Undercoordinated Sites for the Catalysis in Confined Spaces Formed by Two-Dimensional Material Overlayers

Liang Zhang,* May Ling Ng, and Aleksandra Vojvodic*

Cite This: *J. Phys. Chem. Lett.* 2020, 11, 9400−9407

Read Online

ACCESS | Metrics & More | Article Recommendations | SI Supporting Information

ABSTRACT: Adding a two-dimensional (2D) overlayer on a metal surface is a promising route for activating reactants confined in the interfacial space. However, an atomistic understanding of the role played by undercoordinated sites of the 2D overlayer in the activation of molecules in this nanoscaled confined space is yet to be developed. In this paper, we study CO dissociation as a prototypical reaction to investigate CO activation in the confined space enclosed by Rh(111) and a monolayer of hexagonal boron nitride (*h*-BN). The effect of the space size (i.e., the distance between *h*-BN and the metal surface), the type of undercoordinated sites, and the size of the defect are explicitly studied by density functional theory with dispersion correction. The following temperature-programmed X-ray photoelectron spectroscopy measurement suggests that a small portion of the CO dissociated during the desorption, leaving the residual atomic oxygen incorporated into the *h*-BN lattice, which validates the theoretical prediction. The combination of theory and experiment calls for further attention to be paid to the role of undercoordinated sites in the 2D overlayers in confined systems forming potential new catalytic environments.

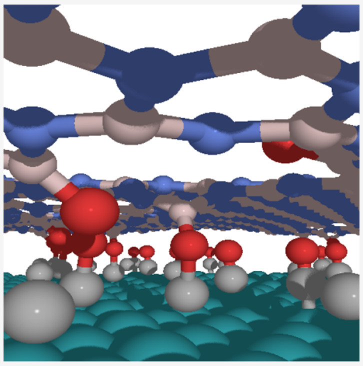

Two-dimensional (2D) materials such as graphene and hexagonal boron nitride (*h*-BN) have attracted tremendous interest because of their unique and tunable electronic and physical properties.[1−10] Both graphene and *h*-BN can be epitaxially grown on different transition metals,[11−19] providing a well-defined interfacial confined space between the 2D monolayer and the metal substrate. For substrates with a good lattice match with the 2D material, such as Ni(111), *h*-BN or graphene can form a 1 × 1 epitaxial overlayer on the metal surface.[19,20] When the lattice mismatch between the substrate and 2D material is large enough, corrugation of these overlayers is then induced to compensate for the strain in the 2D layer, leading to a Morié-type superstructure, which is also known as "nanomesh".[21−23]

It has also been shown that the interfacial confined space between the 2D overlayer and metal surface can be used to capture and confine molecules in an ordered manner. Intercalation of atoms and molecules, such as H, O, H_2, O_2, CO, and H_2O, in graphene[24−28] and *h*-BN[29−32] systems has been studied both experimentally and theoretically. Interestingly, recent studies have shown that chemical reactions can take place in this interfacial confined space with altered activity and selectivity as compared to those of the individual components. For example, Fu and co-workers reported a lower CO oxidation barrier in the confined space of both graphene/Pt(111) and *h*-BN/Pt(111) as compared to that of the bare Pt(111) surface.[33,34] Zhou et al. showed both theoretically and experimentally that the graphene-covered Ni has a rate of hydrogen evolution comparable to that of bare Pt.[35] Ferrighi et al. theoretically predicted an enhanced activity toward O_2 dissociation between anatase TiO_2 and B-doped graphene using hybrid density functional.[36] Datteo et al. reported a prominent cover effect of defective graphene on the dissociation of water that is constrained between the TiO_2 surface and the graphene overlayer.[37] Xiao et al. showed that modulating the chemical potential of reactants through confined space provides an effective route to enhance the catalytic activity.[38,39] A general review of the chemistry and catalysis under the confinement has been given in recent comprehensive surveys by Fu and Bao.[40,41]

Although there have been several efforts to model catalysis in the confined space,[25,28,29,33,36,38,39] a rigorous understanding of how the reactants are activated in the confined space is yet to be developed. Far less discussed is the role of undercoordinated sites in the 2D overlayer and the size of confined space on the chemical transformation in the 2D/metal systems. Therefore, this paper focuses on the overlayer-assisted CO dissociation between the Rh(111) surface and the *h*-BN overlayer by density functional theory (DFT) as a prototypical reaction to understand CO activation in the confined space, especially when associated with undercoordinated sites in the 2D overlayer. CO activation itself is also a critical and often the

Received: August 30, 2020
Accepted: October 13, 2020
Published: October 26, 2020

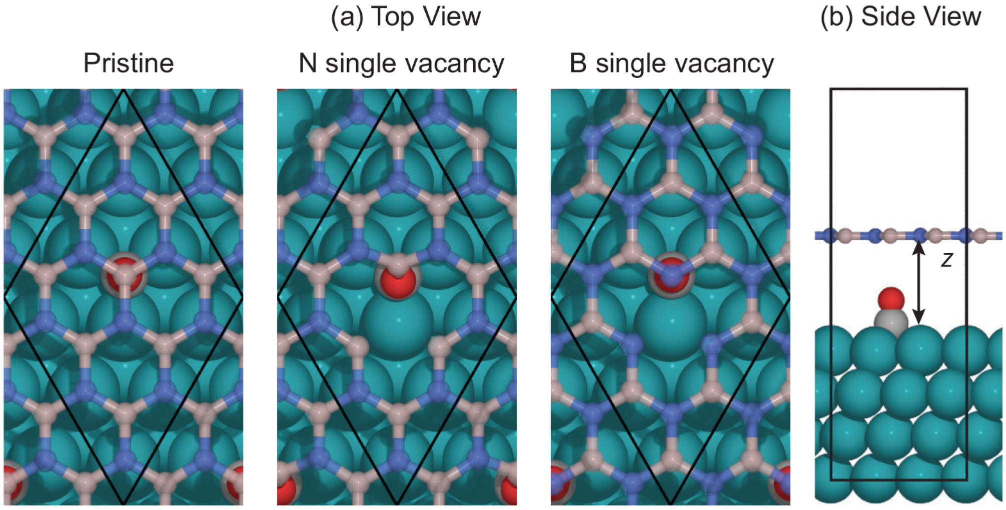

Figure 1. (a) Top view and (b) side view of computational models for CO adsorbed between *h*-BN and Rh(111). Rh, B, C, N, and O are illustrated as green, pink, gray, blue, and red spheres, respectively. The interfacial confined space available for the reaction is defined as the height of *h*-BN above the Rh surface, *z*. The black solid lines highlight the computational supercell.

rate-limiting step in many important chemical processes, such as the methanation reaction and the Fischer−Tropsch synthesis.[42,43] Combining DFT and temperature-programmed X-ray photoelectron spectroscopy (TPXPS), we show that the confinement effect essentially associated with undercoordinated sites in the 2D overlayer is the key for the CO activation between the Rh(111) and *h*-BN overlayer.

We used a simplified p(3 × 3) model in which the *h*-BN plane has been placed relative to a commensurate four-layer Rh(111) lattice. This model allows for a fast computational screening of possible interesting chemistry and is a suitable model for the case in which CO is adsorbed between the *h*-BN overlayer and the surface where the overlayer retains its flatness.[32] The *h*-BN/Rh(111) nanomesh is characterized by "pores" that are ∼2 nm in diameter that interact strongly with the Rh surface and an elevated network of "wires" that interact weakly with the metal. To account for the corrugation effect that is present in reality, we investigate how the nanoscopic chemical environment changes with the distance between the *h*-BN overlayer and the Rh surface by fixing the height of *h*-BN above the metal surface in the *z*-direction (see Figure 1). Because "pores" account for the majority of the nanomesh, the arrangement of Rh, B, and N atoms in the "pore" region was adapted to model the interface, where the N and B atoms are aligned at top and FCC sites, respectively.[44] The bottom two Rh(111) layers were kept frozen, while the rest of the atoms in the system were free to relax. Using this atomic alignment, the calculated equilibrium distance between the *h*-BN overlayer and the Rh(111) surface without CO is 2.2 Å, which is in good agreement with previous reports.[44]

We define the adsorption energy of CO between the *h*-BN and Rh surface at a given distance *z* between them comprising the confined space as follows:

$$E_{\mathrm{ads}}^{\mathrm{CO}}(z) = E_{\mathrm{CO}^*}(z) - E_{h\text{-BN/Rh}}(z) - E_{\mathrm{CO}} \qquad (1)$$

where $E_{\mathrm{CO}^*}(z)$ is the energy of the confined system with intercalated CO at confinement space height *z*, $E_{h\text{-BN/Rh}}(z)$ is the energy of the unintercalated confined system at the same space height, and E_{CO} is the reference energy of a CO molecule. Note that compared to previous studies,[28] where the adsorption energy was referenced to the unintercalated graphene/*h*-BN on metal, the CO adsorption energy in our definition excludes the change of interaction energy between the *h*-BN overlayer and metal surface due to the *z* being different from that of the reference state. Our definition of adsorption energy reflects the real-time CO binding strength in the given confined space, while Andersen's formalism of adsorption energy is referenced to the uninterlaced graphene/*h*-BN at the lowest energy height and better describes the thermodynamics of overall adsorption/desorption. Thus, the adsorption energy defined herein is expected to be stronger than Andersen's formalism.

First, we studied CO adsorption and dissociation under the cover of the pristine *h*-BN overlayer on the Rh(111) surface. It is worth noting that CO does not chemically adsorb on top of a free-standing or Rh-supported pristine *h*- BN monolayer (see Figure S1). In Figure S2, we show the calculated CO adsorption energy for two adsorption sites: fcc and top site for different confinement environments, i.e., different distances *z* between the overlayer and the surface (see Figure 1). Using the scheme of Mason et al.,[45] we obtain the correct site preference for CO adsorption on Rh(111) when the *h*-BN overlayer is far from the surface. The CO adsorption energy on the top site (−1.86 eV) is 0.1 eV stronger than on the fcc site (−1.75 eV). The DFT-calculated equilibrium heights of the *h*-BN overlayer on the Rh(111) surface with CO adsorption on the top and fcc sites are 5.85 and 5.55 Å, respectively. At the equilibrium height distance of 5.5 Å, the CO adsorption energy on the fcc site in the confined space is calculated to be −1.85 eV, which is 0.1 eV stronger than that on the uncovered Rh(111) surface. On the contrary, the *h*-BN overlayer has a weaker effect on the CO adsorption on the top site, where $E_{\mathrm{ads}}^{\mathrm{CO}}$ only changes from −1.85 to −1.90 eV. The preference of the CO adsorption energy on the top over the fcc site decreases from 0.1 to 0.05 eV after adding the *h*-BN overlayer. To confirm the intrinsic change of CO adsorption in the space confined by *h*-BN and Rh described above, we calculated the CO stretching frequency. We find a red shift from 2000.2 to 1990.60 cm^{-1} for the top site and a red shift from 1752.7 to 1741.3 cm^{-1} for the fcc site after adding the *h*-BN overlayer, which is consistent with the enhancement in the CO adsorption energy. A similar ∼17 cm^{-1} red shift in the CO

https://dx.doi.org/10.1021/acs.jpclett.0c02652
J. Phys. Chem. Lett. 2020, 11, 9400−9407

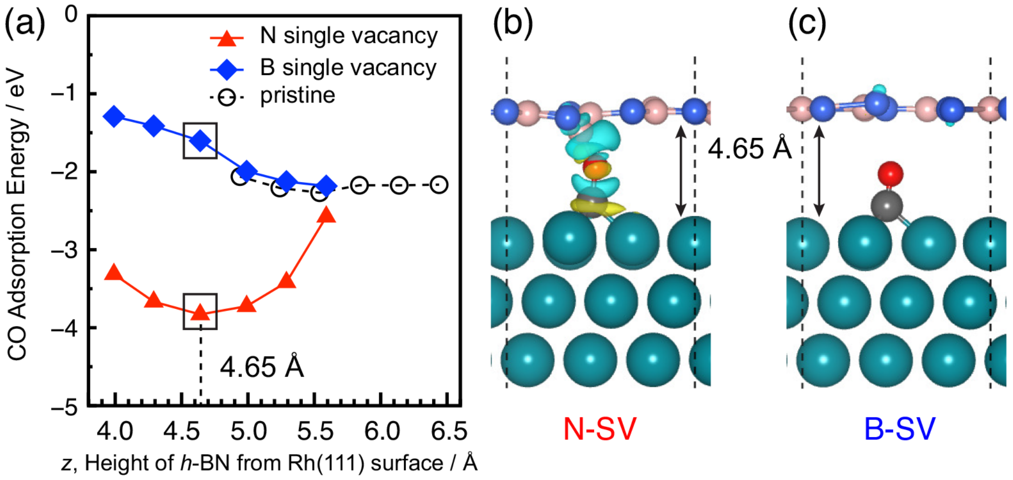

Figure 2. (a) Calculated CO adsorption energy on the FCC site as a function of the z distance between the Rh(111) surface and pristine h-BN (dashed black line), the BN sheet with a single N vacancy (red), and the BN sheet with a single B vacancy (blue). (b and c) Charge density difference of CO adsorbed under N-SV and B-SV for z = 4.65 Å, defined as $\Delta\rho = \rho_{\text{BN/CO-Rh}} - \rho_{\text{BN}} - \rho_{\text{CO-Rh}}$. The isosurface is set to 0.007 e/Å^3, where cyan and yellow represent electron depletion and accumulation, respectively.

stretching frequency has also been observed experimentally in previous studies by Fu et al. on graphene/Pt(111) and h-BN/Pt(111).[33,34] We notice that a weaker CO adsorption energy is reported in the confined space as compared to the uncovered metal surface in the studies mentioned above, which is due to a different choice of reference states as discussed in the definition of adsorption energy.[28] Xiao et al. used confinement energy E_{con} to describe the adsorption energy difference on a cluster when encapsulated in the nanotube and when supported on the out sphere of the nanotube. A consistent positive E_{con} was found. However, the observation may not be directly compared to our results, because the quantum confinement effect on few-atom clusters may not be appliable to extended surfaces.[38]

Notably, when the distance between the h-BN overlayer and the surface is <5.5 Å, the top site becomes unstable and the CO molecule exhibits a spontaneous change in site to the nearby fcc site. Therefore, we chose the fcc site as the initial adsorption geometry for our study of the CO dissociation process. This choice also allows for a study of a wider range of z of the h-BN above the surface. However, we expect our findings to be applicable to other binding sites, e.g., the top site.

We next examined h-BN-assisted CO dissociation between the pristine h-BN overlayer and Rh(111), where the dissociated C atom remains on the Rh(111) surface and the O atom settles on the h-BN overlayer separately. Figure S2 shows the calculated reaction barriers for overlayer-assisted CO dissociation at the FCC site and its dependence on the distance between the pristine h-BN overlayer and Rh surface. We find prohibitively high CO dissociation barriers for all z values. At the equilibrium height (z = 5.5 Å), the calculated CO dissociation barrier for the overlayer-assisted mechanism is 4.5 eV (see Figure S3), which is significantly higher than the conventional CO dissociation barrier on the uncovered Rh(111) surface (~3.2 eV),[46,47] shown as the red dashed line in Figure S2. Although the CO dissociation barrier decreases with confinement space (smaller z values), we find that the dissociation barrier is always higher than the CO adsorption energy; in other words, the decrease in the activation energy is not sufficient to make the dissociation process feasible before the desorption of CO from the Rh(111) surface. Hence, we conclude that a pristine h-BN overlayer can hardly activate dissociation in the confined space. Notably, it is well accepted that the conventional CO dissociation on transitional metal surfaces is unlikely to occur before CO desorption on Rh(111).[48]

h-BN sheets are normally prepared in experiments through electron beam irradiation,[49,50] chemical vapor deposition, etc.[51,52] Various defects with different sizes can be produced due to the radiation damage, the misalignment of the random nucleation centers, as evidenced by scanning tunneling microscopy (STM),[32,52] and high-resolution transmission electron microscopy.[49,50] Despite their abundant presence, the role of these vacancies in the chemistry in the confined space is not well understood. In this paper, our investigation starts with a simple vacancy model, i.e., a single vacancy. There are two possible single-vacancy geometries: N single vacancy (N-SV) and B single vacancy (B-SV). In the single-vacancy model, one N or one B atom is removed from the h-BN lattice, resulting in a local atomic arrangement with three undercoordinated B or N atoms, respectively. As illustrated in Figure 1, CO dissociation at the FCC site under N-SV and B-SV is studied for different h-BN heights, where CO is placed directly below the undercoordinated B or N atom. To make a fair comparison, for the B-SV model, B and N atoms are switched with each other and CO remains at the FCC adsorption site with an undercoordinated N atom on top. Such a change in the B and N arrangement causes a change in the van der Waals interaction of only <0.02 eV between the h-BN sheet and Rh(111) surface at a height of 4.65 Å.

Figure 2 shows how the presence of N-SV significantly enhances CO binding in the confined space, resulting in an equilibrium height z of 4.65 Å between h-BN and the surface that is downshifted compared to a z of 5.5 Å for the system with pristine h-BN. The C−O bond length of the CO under N-SV is also elongated from 1.19 to 1.31 Å as compared to the one on the uncovered surface, which could be a sign of the activation of the C−O bond. Such enhancement in CO binding is a consequence of the interaction between the O atom and the undercoordinated B atom. A Bader charge analysis of the system at the equilibrium z of 4.65 Å suggests a

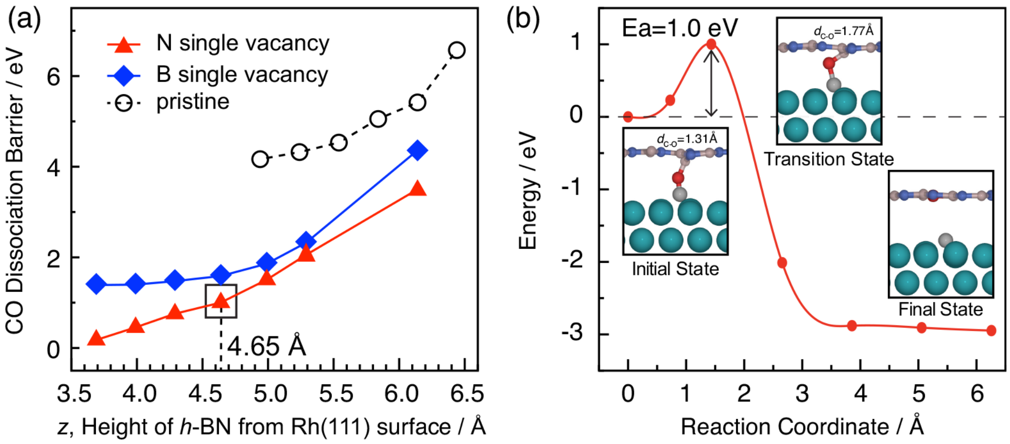

Figure 3. (a) Calculated *h*-BN-assisted CO dissociation barriers as a function of distance *z* between the Rh(111) surface and a *h*-BN sheet with a N (red) or B (blue) single vacancy. For comparison, the dissociation barriers under a pristine *h*-BN sheet are also shown with empty circles. (b) Minimal energy path of N-SV *h*-BN-assisted CO dissociation at the equilibrium *z* of 4.65 Å (boxed point in panel a), with a side view of the corresponding initial, transition, and final states.

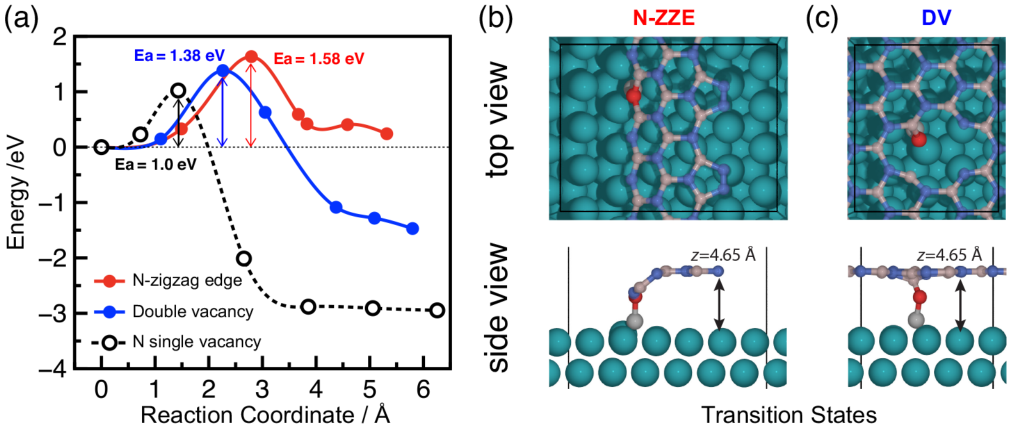

Figure 4. (a) Calculated dissociation energetics of confined CO between Rh(111) and undercoordinated B atom of the N single vacancy (N-SV), the double vacancy (DV), and the N-terminated zigzag edge (N-ZZE) of the *h*-BN overlayer at a *z* of 4.65 Å. (b and c) Top views and side views of the corresponding transition states of CO dissociation between Rh(111) and the N-terminated zigzag edge (N-ZZE) and the double vacancy (DV), respectively. The transition state of N-SV model is given in Figure 3b.

charge transfer of 0.75e from the undercoordinated B atom above the CO is distributed to the adsorbed CO molecule ($\Delta\rho_O$ = 0.6e, and $\Delta\rho_C$ = 0.15e). The presence of the charge transfer is visualized in Figure 2b, which shows the calculated differential charge density in real space, defined as $\Delta\rho = \rho_{BN/CO\text{-}Rh} - \rho_{BN} - \rho_{CO\text{-}Rh}$. On the contrary, CO adsorption under B-SV is much weaker than N-SV and exhibits a trend similar to that of the pristine *h*-BN. A Bader charge analysis of this system shows that there is almost no charge transferred from B-SV in the *h*-BN to the adsorbed CO, which is also evidenced by the differential charge density plot in Figure 2c. We hence conclude that the presence of the right type of vacancy can result in a more preferential CO chemistry in the confined space as compared to the uncovered Rh surface.

When it comes to CO dissociation in the presence of a single vacancy in the *h*-BN sheet on Rh(111), we find that both B-SV and N-SV reduce the CO dissociation barrier significantly (see Figure 3). For a given *z* value of the separation between the *h*-BN and the surface, the N-SV is always more reactive toward CO dissociation than the B-SV. The decrease in the CO dissociation barrier for the N-SV system originates from the stronger B−O interaction, which substantially stabilizes the transition state. We find that the CO dissociation barriers in the N-SV and B-SV systems are significantly smaller than those of pristine *h*-BN/Rh(111), suggesting a more pronounced activity. For the optimal *z* value of 4.65 Å (highlighted in Figures 2 and 3), where confined CO has the strongest binding, a barrier of only 1.0 eV is needed for CO to dissociate for the N-SV system. This barrier is much smaller than the CO dissociation barrier (∼3.2 eV) on the uncovered Rh(111) surface and compatible to the barrier on the stepped Rh(211) surface (∼2.0 eV).[53] This relatively small CO dissociation barrier indicates that some amount of CO is dissociated below 600 K and the dissociated O atom forms a B−O bond in the *h*-BN lattice. Our analysis of the single-vacancy systems suggests that the undercoordinated B atom in the vicinity of a N vacancy in the *h*-BN overlayer is a potential reactive center for low-temperature CO dissociation. Undercoordinated N sites are less active than undercoordinated B sites in terms of both adsorption energy and dissociation barrier, due to the weaker N−O interaction than B−O interaction. Therefore, only undercoordinated B sites are considered in the following discussion. However, a similar size dependency was also found for undercoordinated N sites (Figure S7).

The single-layer *h*-BN sheet has undercoordinated B atoms in defects of different sizes during its synthesis, from a point defect (single vacancy) to the edge of clusters. The electronic structure and catalytic properties of undercoordinated B atoms can depend on the size of the defect and the local chemical environment. Here, we go beyond the single-vacancy model in the discussion presented above and investigate *h*-BN-assisted CO activation as a function of the defect size, including the dissociation of intercalated CO below undercoordinated B atoms of a double vacancy (DV) and an N-terminated zigzag edge (N-ZZE), as illustrated in Figure 4. Notably, the N-ZZE has been found to be one of the most energetically stable edges of *h*-BN clusters[54,55] and is also a good representation of infinite large defects. Due to the size of the simulation cell needed for the larger defect models, we model the *h*-BN at a fixed distance above the Rh surface (z = 4.65 Å) and compare these results to the N-SV vacancy model.

Figure 4 compares the CI-NEB-calculated minimum energy paths for CO dissociation under three different defects of *h*-BN on the Rh surface: N-SV, DV, and N-ZZE. These three defect models probe different types of undercoordinated B atoms as potential reactive sites for the dissociation. We find that as the size of the vacancy increases, the product state energies relative to the reactant state are dramatically increased by ∼3.2 eV from N-SV to N-ZZE. In other words, the binding between the residual O atom, originating from the dissociated CO, and the defect of the *h*-BN overlayer is weakened as the vacancy increases in size. Meanwhile, there is a much smaller upshift (0.58 eV) of the transition state energies. The reaction coordinates of the transition states indicate that the transition state closely resembles the reactant state (CO adsorbed between undercoordinated B atoms and Rh surface) when the defect size is small and shifts away from the reactant structure toward the product structure when the size of the defect increases. Table 1 summarizes the binding energies of CO between Rh and *h*-BN ($E_{\mathrm{ads}}^{\mathrm{CO}}$), the *h*-BN-assisted CO dissociation barrier (E_{a}), the residual O binding energy ($E_{\mathrm{ads}}^{\mathrm{O@def}}$), and the CO binding energy ($E_{\mathrm{ads}}^{\mathrm{CO@def}}$) to the defect of the *h*-BN overlayer for the three vacancy models at a fixed height of *h*-BN of 4.65 Å above the Rh surface. Although the lowest CO dissociation barrier is found for the N-SV system, the fact that CO and O bind more strongly to the defect ($E_{\mathrm{ads}}^{\mathrm{CO@def}}$ and $E_{\mathrm{ads}}^{\mathrm{O@def}}$) as compared to the CO binding between Rh and *h*-BN suggests that N-SV can be easily poisoned by a CO molecule or residual O atom. On the contrary, the larger vacancies exhibit a better trade-off between the CO dissociation activation barrier and resistance to poisoning and could therefore play a critical role in CO activation in the confined space between *h*-BN and Rh(111).

Table 1. Calculated CO Binding Energies between Rh and *h*-BN ($E_{\mathrm{ads}}^{\mathrm{CO}}$) and on the Vacancy of the *h*-BN Lattice ($E_{\mathrm{ads}}^{\mathrm{CO@def}}$), CO Dissociation Barriers (E_{a}), and Residual O Binding Energies ($E_{\mathrm{ads}}^{\mathrm{O@def}}$) on the Vacancy of the *h*-BN Lattice of Different Vacancy Models at the *h*-BN Height of 4.65 Å[a]

	$E_{\mathrm{ads}}^{\mathrm{CO}}$	E_{a}	$E_{\mathrm{ads}}^{\mathrm{CO@def}}$	$E_{\mathrm{ads}}^{\mathrm{O@def}}$
N-SV	−3.83	1.00	−3.98	−6.75
DV	−2.79	1.38	−2.57	−4.99
N-ZZE	−2.35	1.58	−0.55	−2.67

[a] Corresponding geometries of intercalated CO, CO@def, and O@def can be found in Figures S4−S6.

Figure 5 shows the 2D C 1s and O 1s photoelectron spectra of CO intercalated in *h*-BN/Rh(111) and adsorbed on the uncovered Rh(111) surface for temperatures from 320 to 850 K. There are two distinct features of the TPXPS. First, the most interesting finding is the O feature above 600 K. The binding energy of 532 eV suggests the formation of a B−O bond,[56] which strongly indicates that small amounts of CO are dissociated between *h*-BN and Rh(111) at low temperatures with dissociated O remaining in the *h*-BN overlayer. A similar O 1s feature was also observed by Meng et al., where *h*-BN/Pt(111) was exposed to a mild oxidation environment in O_2 or NO_2.[57] Second, the completion temperature of CO desorption is higher for the *h*-BN overlayer/Rh system (top, 605 K; hollow, 575 K) than for the uncovered Rh surface (top, 480 K; hollow, 400 K). For *h*-BN overlayer/Rh, we find a smaller desorption temperature difference between the TOP site and the FCC site (ΔT = 30 K for *h*-BN/Rh, and ΔT = 80 K for Rh). Although the change in CO desorption temperature could be due to the diffusion kinetics under confinement, it is also in line with our calculated CO adsorption energetics as shown in Figure S2, where the differences in the CO adsorption energy on the TOP site and FCC site are reduced by 0.05 eV after adding the *h*-BN cover.

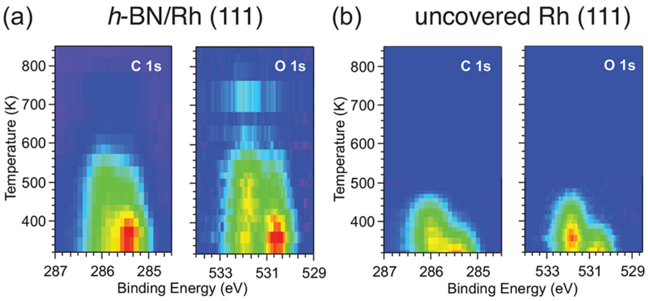

Figure 5. Photoemission spectra of (a) C 1s and O 1s orbitals as a function of temperature for CO intercalated in *h*-BN/Rh(111) and (b) CO adsorbed on uncovered Rh(111).

Our calculations suggest that a *h*-BN-assisted CO dissociation mechanism, where CO molecules bind between an undercoordinated B atom and the Rh(111), is feasible for dissociation under experimental conditions. The dissociation barriers of the three different vacancy models we explored are all lower or comparable to the CO desorption energy. The B−O feature in the O 1s photoelectron spectra can be explained well by the incorporation of the residual O atom into the *h*-BN defect sites. Furthermore, the fact that the B−O feature diminishes after 800 K indicates that the observed CO dissociation occurs at relatively larger defect sites where the binding of O to the defect is moderate. It should be noted that the B−O feature cannot be explained by the conventional CO dissociation mechanism on a transition metal surface for the following two reasons. (1) It is well accepted that the conventional CO dissociation on transition metal surfaces is unlikely to occur before CO desorption on Rh(111),[48] which is also consistent with our DFT calculation shown in Figure S2, where the conventional CO dissociation barrier is found to be 1.0 eV higher than the CO desorption energy (CO adsorption energy with the opposite sign). (2) A previous TPD study of

O/Rh(111) revealed that O desorption from a Rh(111) surface requires a temperature higher than 1000 K at an O coverage of <0.1 monolayer.[58−60] Therefore, even if CO dissociation takes place at steps of a Rh surface without the direct assistance of *h*-BN, it is still unlikely that the dissociated O atoms desorb from the Rh surface and incorporate *h*-BN defect sites below 600 K. In summary, the TPXPS experiments support not only the calculated CO adsorption and dissociation energetics but also the finding that dissociation of intercalated CO in the confined space between *h*-BN and the Rh surface is associated with undercoordinated B atoms in the vacancies of the *h*-BN overlayer.

To conclude, we have compared the CO chemistry on an uncovered Rh(111) surface with that confined by a *h*-BN overlayer. DFT calculations revealed that CO dissociation is prohibited under a pristine *h*-BN overlayer on Rh(111). Using a simple single-vacancy model, we found that undercoordinated B atoms have substantially stronger CO affinity than pristine *h*-BN or undercoordinated N atoms and are responsible for the *h*-BN-assisted CO activation. Larger vacancy models revealed that undercoordinated B atoms at large size vacancies or edges have better stability and higher resistance toward CO and O poisoning, with only a slight change in the dissociation barrier. We further performed TPXPS measurements showing that desorption of intercalated CO from the confined space in the *h*-BN/Rh exhibits an unusual O 1s peak after CO desorption. This feature can be explained only by the undercoordinated B atom-assisted CO dissociation and formation of a B−O bond in the *h*-BN overlayer. Therefore, both theory and experiment suggest that CO can be activated only with undercoordinated B atoms of the *h*-BN overlayer. We also expect that a similar effect can also be achieved by p-type doped graphene in a controlled manner. Our findings suggest that a pristine 2D overlayer has a very small effect in activating CO. However, vacancies, edges, or doping of the 2D overlayer could have a strong impact on the reactivity and selectivity of the chemical transformations in the confined system and deserve more attention. From a practical point of view, this study implies that increasing the undercoordinated B sites in the 2D overlayer through proper defect engineering could efficiently improve the activation of CO in the confined space, which sheds light on a new strategy of designing 2D material-covered catalytic systems for relevant catalytic processes, such as the syngas conversion reactions.

DFT was used to calculate all energeitcs, using the Vienna *ab initio* simulation package.[61,62] Core electrons were described using the projector-augmented wave method.[63,64] Kohn−Sham single-electron wave functions were expanded in a plane wave basis with a kinetic energy cutoff of 400 eV to describe the valence electrons. A nonlocal van der Waals density functional (vdW-DF), optB88-vdW, was chosen for better treatment of long-range dispersion.[65,66] Geometries were considered optimized when the force on each atom was <0.01 eV/Å. All of the transition states were calculated with the climbing-image nudged elastic band method (CI-NEB).[67,68] Bader's atoms-in-molecules approach was used to quantify changes in atomic charges of CO molecules under different confinement environments.[69,70]

TPXPS experiments were performed at beamline 11.0.2 of the Advanced Light Source (Berkeley, CA). The Rh(111) single-crystal surface was cleaned by several cycles of Ar^+ sputtering and annealing up to 1200 K. The surface was considered clean when no contaminants were detected by XPS. The *h*-BN monolayer was prepared by thermal cracking of borazine using the procedure described previously.[21] The quality of the *h*-BN layer was checked through the XPS N 1s spectra.[14] CO adsorption on the Rh(111) surface and CO intercalation in the *h*-BN/Rh system at room temperature were achieved according to the procedure described in ref 32. TPXPS of CO adsorbed on Rh(111) and CO intercalated in the *h*-BN/Rh system was performed by heating the system from the back of the single crystal at a temperature increment rate of 10 K/min while accumulating successive C and O 1s spectra using a fixed excitation photon energy of 730 eV. Precautions were taken to avoid beam damage by taking spectra in only the essential energy range and by moving to a new beam exposure spot before the onset of beam damage. All spectra were normalized to the pre-core level background.

■ ASSOCIATED CONTENT

Supporting Information

The Supporting Information is available free of charge at https://pubs.acs.org/doi/10.1021/acs.jpclett.0c02652.

> CO adsorption above *h*-BN, CO adsorption and dissociation under the pristine *h*-BN cover, MEP of pristine h-BN-assisted CO dissociation, CO adsorption under the unsaturated B sites of different defects, CO and O adsorption at the defect site,and MEP of CO dissociation under the unsaturated N sites of the double vacancy (PDF)

■ AUTHOR INFORMATION

Corresponding Authors

Liang Zhang − *Center for Combustion Energy, School of Vehicle and Mobility, and State Key Laboratory of Automotive Safety and Energy, Tsinghua University, Beijing 100084, China;* orcid.org/0000-0002-9718-0436; Email: zhangbright@tsinghua.edu.cn

Aleksandra Vojvodic − *Department of Chemical and Biomolecular Engineering, University of Pennsylvania, Philadelphia, Pennsylvania 19104-6315, United States;* orcid.org/0000-0002-5584-6711; Email: alevoj@seas.upenn.edu

Author

May Ling Ng − *SLAC National Accelerator Laboratory, Stanford University, Menlo Park, California 94025, United States*

Complete contact information is available at: https://pubs.acs.org/10.1021/acs.jpclett.0c02652

Notes

The authors declare no competing financial interest.

■ ACKNOWLEDGMENTS

A.V. acknowledges the Canadian Institute for Advanced Research (CIFAR) for support through the Bioinspired Solar Energy Program. The authors acknowledge the use of computer time allocation at the National Energy Research Scientific Computing Center (NERSC), a U.S. Department of Energy (DOE) Office of Science User Facility supported by the Office of Science of the DOE under Contract DE-AC02-05CH1123.

REFERENCES

(1) Berger, C. Electronic Confinement and Coherence in Patterned Epitaxial Graphene. *Science* **2006**, *312*, 1191−1196.

(2) Geim, A. K.; Novoselov, K. S. The Rise of Graphene. *Nat. Mater.* **2007**, *6*, 183−191.

(3) Geim, A. K. Graphene: Status and Prospects. *Science* **2009**, *324*, 1530−1534.

(4) Xia, F.; Mueller, T.; Lin, Y.-m.; Valdes-Garcia, A.; Avouris, P. Ultrafast Graphene Photodetector. *Nat. Nanotechnol.* **2009**, *4*, 839−843.

(5) Chopra, N. G.; Luyken, R. J.; Cherrey, K.; Crespi, V. H.; Cohen, M. L.; Louie, S. G.; Zettl, A. Boron Nitride Nanotubes. *Science* **1995**, *269*, 966−967.

(6) Jin, C.; Lin, F.; Suenaga, K.; Iijima, S. Fabrication of a Freestanding Boron Nitride Single Layer and Its Defect Assignments. *Phys. Rev. Lett.* **2009**, *102*, 195505.

(7) Zeng, H.; Zhi, C.; Zhang, Z.; Wei, X.; Wang, X.; Guo, W.; Bando, Y.; Golberg, D. White Graphenes": Boron Nitride Nanoribbons via Boron Nitride Nanotube Unwrapping. *Nano Lett.* **2010**, *10*, 5049−5055.

(8) Song, L.; Ci, L.; Lu, H.; Sorokin, P. B.; Jin, C.; Ni, J.; Kvashnin, A. G.; Kvashnin, D. G.; Lou, J.; Yakobson, B. I.; et al. Large Scale Growth and Characterization of Atomic Hexagonal Boron Nitride Layers. *Nano Lett.* **2010**, *10*, 3209−3215.

(9) Nag, A.; Raidongia, K.; Hembram, K. P. S. S.; Datta, R.; Waghmare, U. V.; Rao, C. N. R. Graphene Analogues of BN: Novel Synthesis and Properties. *ACS Nano* **2010**, *4*, 1539−1544.

(10) Golberg, D.; Bando, Y.; Huang, Y.; Terao, T.; Mitome, M.; Tang, C.; Zhi, C. Boron Nitride Nanotubes and Nanosheets. *ACS Nano* **2010**, *4*, 2979−2993.

(11) Goriachko, A.; He, Y.; Knapp, M.; Over, H.; Corso, M.; Brugger, T.; Berner, S.; Osterwalder, J.; Greber, T. Self-Assembly of a Hexagonal Boron Nitride Nanomesh on Ru(0001). *Langmuir* **2007**, *23*, 2928−2931.

(12) Laskowski, R.; Blaha, P. Ab Initio Study of h-BN Nanomeshes on Ru(001), Rh(111), and Pt(111). *Phys. Rev. B: Condens. Matter Mater. Phys.* **2010**, *81*, 075418.

(13) Laskowski, R.; Blaha, P.; Schwarz, K. Bonding of Hexagonal BN to Transition Metal Surfaces: An Ab Initio Density-functional Theory Study. *Phys. Rev. B: Condens. Matter Mater. Phys.* **2008**, *78*, 045409.

(14) Preobrajenski, A.; Nesterov, M.; Ng, M. L.; Vinogradov, A.; Mårtensson, N. Monolayer h-BN on Lattice-mismatched Metal Surfaces: On the Formation of the Nanomesh. *Chem. Phys. Lett.* **2007**, *446*, 119−123.

(15) Brugger, T.; Günther, S.; Wang, B.; Dil, J. H.; Bocquet, M.-L.; Osterwalder, J.; Wintterlin, J.; Greber, T. Comparison of Electronic Structure and Template Function of Single-Layer Graphene and a Hexagonal Boron Nitride Nanomesh on Ru(0001). *Phys. Rev. B: Condens. Matter Mater. Phys.* **2009**, *79*, 045407.

(16) Müller, F.; Hüfner, S.; Sachdev, H.; Laskowski, R.; Blaha, P.; Schwarz, K. Epitaxial Growth of Hexagonal Boron Nitride on Ag(111). *Phys. Rev. B: Condens. Matter Mater. Phys.* **2010**, *82*, 113406.

(17) Čavar, E.; Westerström, R.; Mikkelsen, A.; Lundgren, E.; Vinogradov, A.; Ng, M. L.; Preobrajenski, A.; Zakharov, A.; Mårtensson, N. A Single h-BN Layer on Pt(111). *Surf. Sci.* **2008**, *602*, 1722−1726.

(18) Morscher, M.; Corso, M.; Greber, T.; Osterwalder, J. Formation of Single Layer h-BN on Pd(111). *Surf. Sci.* **2006**, *600*, 3280−3284.

(19) Preobrajenski, A.; Vinogradov, A.; Mårtensson, N. Monolayer of h-BN Chemisorbed on Cu(111) and Ni(111): The Role of the Transition Metal 3d States. *Surf. Sci.* **2005**, *582*, 21−30.

(20) Shimoyama, I.; Baba, Y.; Sekiguchi, T.; Nath, K. A. Theoretical Interpretation of Near Edge X-Ray Absorption Fine Structure of Hexagonal Boron Nitride Monolayer on Ni(111). *J. Electron Spectrosc. Relat. Phenom.* **2009**, *175*, 6−13.

(21) Preobrajenski, A. B.; Vinogradov, A. S.; Ng, M. L.; Ćavar, E.; Westerström, R.; Mikkelsen, A.; Lundgren, E.; Mårtensson, N. Influence of Chemical Interaction at the Lattice-mismatched h-BN/Rh(111) and h-BN/Pt(111) Interfaces on the Overlayer Morphology. *Phys. Rev. B: Condens. Matter Mater. Phys.* **2007**, *75*, 245412.

(22) Preobrajenski, A. B.; Ng, M. L.; Vinogradov, A. S.; Mårtensson, N. Controlling Graphene Corrugation on Lattice-mismatched Substrates. *Phys. Rev. B: Condens. Matter Mater. Phys.* **2008**, *78*, 073401.

(23) Corso, M.; Auwärter, W.; Muntwiler, M.; Tamai, A.; Greber, T.; Osterwalder, J. Boron Nitride Nanomesh. *Science* **2004**, *303*, 217−220.

(24) Zhang, H.; Fu, Q.; Cui, Y.; Tan, D.; Bao, X. Growth Mechanism of Graphene on Ru(0001) and O_2 Adsorption on the Graphene/Ru(0001) Surface. *J. Phys. Chem. C* **2009**, *113*, 8296−8301.

(25) Grånäs, E.; Knudsen, J.; Schröder, U. A.; Gerber, T.; Busse, C.; Arman, M. A.; Schulte, K.; Andersen, J. N.; Michely, T. Oxygen Intercalation under Graphene on Ir(111): Energetics, Kinetics, and the Role of Graphene Edges. *ACS Nano* **2012**, *6*, 9951−9963.

(26) Feng, X.; Maier, S.; Salmeron, M. Water Splits Epitaxial Graphene and Intercalates. *J. Am. Chem. Soc.* **2012**, *134*, 5662−5668.

(27) Grånäs, E.; Andersen, M.; Arman, M. A.; Gerber, T.; Hammer, B.; Schnadt, J.; Andersen, J. N.; Michely, T.; Knudsen, J. CO Intercalation of Graphene on Ir(111) in the Millibar Regime. *J. Phys. Chem. C* **2013**, *117*, 16438−16447.

(28) Andersen, M.; Hornekær, L.; Hammer, B. Understanding Intercalation Structures Formed Under Graphene on Ir(111). *Phys. Rev. B: Condens. Matter Mater. Phys.* **2014**, *90*, 155428.

(29) Brugger, T.; Ma, H.; Iannuzzi, M.; Berner, S.; Winkler, A.; Hutter, J.; Osterwalder, J.; Greber, T. Nanotexture Switching of Single-Layer Hexagonal Boron Nitride on Rhodium by Intercalation of Hydrogen Atoms. *Angew. Chem., Int. Ed.* **2010**, *49*, 6120−6124.

(30) Ding, Y.; Iannuzzi, M.; Hutter, J. Investigation of Boron Nitride Nanomesh Interacting with Water. *J. Phys. Chem. C* **2011**, *115*, 13685−13692.

(31) Ding, Y.; Iannuzzi, M.; Hutter, J. Investigation of h-BN/Rh(111) Nanomesh Interacting With Water and Atomic Hydrogen. *Chimia* **2011**, *65*, 256−259.

(32) Ng, M. L.; Shavorskiy, A.; Rameshan, C.; Mikkelsen, A.; Lundgren, E.; Preobrajenski, A.; Bluhm, H. Reversible Modification of the Structural and Electronic Properties of a Boron Nitride Monolayer by CO Intercalation. *ChemPhysChem* **2015**, *16*, 923−927.

(33) Yao, Y.; Fu, Q.; Zhang, Y. Y.; Weng, X.; Li, H.; Chen, M.; Jin, L.; Dong, A.; Mu, R.; Jiang, P.; et al. Graphene Cover-Promoted Metal-Catalyzed Reactions. *Proc. Natl. Acad. Sci. U. S. A.* **2014**, *111*, 17023−17028.

(34) Zhang, Y.; Weng, X.; Li, H.; Li, H.; Wei, M.; Xiao, J.; Liu, Z.; Chen, M.; Fu, Q.; Bao, X. Hexagonal Boron Nitride Cover on Pt(111): A New Route to Tune Molecule−Metal Interaction and Metal-Catalyzed Reactions. *Nano Lett.* **2015**, *15*, 3616−3623.

(35) Zhou, Y.; Chen, W.; Cui, P.; Zeng, J.; Lin, Z.; Kaxiras, E.; Zhang, Z. Enhancing the Hydrogen Activation Reactivity of Nonprecious Metal Substrates via Confined Catalysis Underneath Graphene. *Nano Lett.* **2016**, *16*, 6058−6063.

(36) Ferrighi, L.; Datteo, M.; Fazio, G.; Di Valentin, C. Catalysis under Cover: Enhanced Reactivity at the Interface between (Doped) Graphene and Anatase TiO_2. *J. Am. Chem. Soc.* **2016**, *138*, 7365−7376.

(37) Datteo, M.; Liu, H.; Di Valentin, C. Water on Graphene-Coated TiO_2: Role of Atomic Vacancies. *ACS Appl. Mater. Interfaces* **2018**, *10*, 5793−5804.

(38) Xiao, J.; Pan, X.; Guo, S.; Ren, P.; Bao, X. Toward Fundamentals of Confined Catalysis in Carbon Nanotubes. *J. Am. Chem. Soc.* **2015**, *137*, 477−482.

(39) Guo, C.; Xiao, J. Towards Unifying the Concepts of Catalysis in Confined Space. *Comput. Mater. Sci.* **2019**, *161*, 58−63.

(40) Fu, Q.; Bao, X. Catalysis on a Metal Surface With a Graphitic Cover. *Chinese Journal of Catalysis* **2015**, *36*, 517−519.

(41) Fu, Q.; Bao, X. Surface Chemistry and Catalysis Confined Under Two-Dimensional Materials. *Chem. Soc. Rev.* **2017**, *46*, 1842−1874.

(42) Sachtler, W. M. H.; Ichikawa, M. Catalytic Site Requirements for Elementary Steps in Syngas Conversion to Oxygenates over Promoted Rhodium. *J. Phys. Chem.* **1986**, *90*, 4752.

(43) de Koster, A.; van Santen, R. A. Dissociation of CO on Rh Surfaces. *Surf. Sci.* **1990**, *233*, 366−380.

(44) Laskowski, R.; Blaha, P.; Gallauner, T.; Schwarz, K. Single-Layer Model of the Hexagonal Boron Nitride Nanomesh on the Rh(111) Surface. *Phys. Rev. Lett.* **2007**, *98*, 106802.

(45) Mason, S. E.; Grinberg, I.; Rappe, A. M. First-Principles Extrapolation Method for Accurate CO Adsorption Energies on Metal Surfaces. *Phys. Rev. B: Condens. Matter Mater. Phys.* **2004**, *69*, 161401.

(46) Mavrikakis, M.; Bäumer, M.; Freund, H.-J.; Nørskov, J. Structure Sensitivity of CO Dissociation on Rh Surfaces. *Catal. Lett.* **2002**, *81*, 153−156.

(47) Liu, Z.-P.; Hu, P. General Trends in CO Dissociation on Transition Metal Surfaces. *J. Chem. Phys.* **2001**, *114*, 8244−8247.

(48) Yates, J.; Williams, E.; Weinberg, W. Reply To Comments on "Does Chemisorbed Carbon Monoxide Dissociate on Rhodium?" by D.G. Castner, L.H. Dubois, B.A. Sexton and G.A. Somorjai. *Surf. Sci.* **1982**, *115*, L93−L95.

(49) Jin, C.; Lin, F.; Suenaga, K.; Iijima, S. Fabrication of a Freestanding Boron Nitride Single Layer and Its Defect Assignments. *Phys. Rev. Lett.* **2009**, *102*, 195505.

(50) Meyer, J. C.; Chuvilin, A.; Algara-Siller, G.; Biskupek, J.; Kaiser, U. Selective Sputtering and Atomic Resolution Imaging of Atomically Thin Boron Nitride Membranes. *Nano Lett.* **2009**, *9*, 2683−2689.

(51) Shi, Y.; Hamsen, C.; Jia, X.; Kim, K. K.; Reina, A.; Hofmann, M.; Hsu, A. L.; Zhang, K.; Li, H.; Juang, Z.-Y.; et al. Synthesis of Few-Layer Hexagonal Boron Nitride Thin Film by Chemical Vapor Deposition. *Nano Lett.* **2010**, *10*, 4134−4139.

(52) Auwärter, W.; Suter, H. U.; Sachdev, H.; Greber, T. Synthesis of One Monolayer of Hexagonal Boron Nitride on Ni(111) from B-Trichloroborazine $(ClBNH)_3$. *Chem. Mater.* **2004**, *16*, 343−345.

(53) Wang, S.; Temel, B.; Shen, J.; Jones, G.; Grabow, L. C.; Studt, F.; Bligaard, T.; Abild-Pedersen, F.; Christensen, C. H.; Nørskov, J. K. Universal Brønsted-Evans-Polanyi Relations for C−C, C−O, C−N, N−O, N−N, and O−O Dissociation Reactions. *Catal. Lett.* **2011**, *141*, 370−373.

(54) Fu, X.; Zhang, R. Energetics of Hexagonal Boron Nitride Nanostructures: Edge Dependence and Truncation Effects. *Nanoscale* **2017**, *9*, 6734−6740.

(55) Gomes, L. C.; Alexandre, S. S.; Chacham, H.; Nunes, R. W. Stability of Edges and Extended Defects on Boron Nitride and Graphene Monolayers: The Role of Chemical Environment. *J. Phys. Chem. C* **2013**, *117*, 11770−11779.

(56) Seal, S.; Barr, T. L.; Sobczak, N.; Benko, E. X-ray Photoelectron Spectroscopy Study of the Chemical Interaction Between BN and Ti/TiN. *J. Vac. Sci. Technol., A* **1997**, *15*, 505−512.

(57) Meng, C.; Li, Y.; Wu, H.; Wei, W.; Ning, Y.; Cui, Y.; Fu, Q.; Bao, X. Structural Transformation of *h*-BN Overlayers on Pt(111) in Oxidative Atmospheres. *Phys. Chem. Chem. Phys.* **2018**, *20*, 11013−11020.

(58) Xu, X.; Friend, C. M. Partial Oxidation without Allylic Carbon-Hydrogen Bond Activation: the Conversion of Propene to Acetone on Rhodium(111)-p(2 × 1)-O. *J. Am. Chem. Soc.* **1991**, *113*, 6779−6785.

(59) Root, T.; Schmidt, L.; Fisher, G. B. Adsorption and Reaction of Nitric Oxide and Oxygen on Rh(111). *Surf. Sci.* **1983**, *134*, 30−45.

(60) Franz, T.; Mittendorfer, F. Kinetic Monte Carlo Simulations of Temperature Programed Desorption of O/Rh(111). *J. Chem. Phys.* **2010**, *132*, 194701.

(61) Kresse, G.; Hafner, J. First-principles Study of the Adsorption of Atomic H on Ni (111), (100) and (110). *Surf. Sci.* **2000**, *459*, 287−302.

(62) Kresse, G. Dissociation and sticking of H_2 on the Ni(111), (100), and (110) substrate. *Phys. Rev. B: Condens. Matter Mater. Phys.* **2000**, *62*, 8295−8305.

(63) Blöchl, P. E. ProjectoR Augmented-Wave Method. *Phys. Rev. B: Condens. Matter Mater. Phys.* **1994**, *50*, 17953−17979.

(64) Kresse, G.; Joubert, D. From Ultrasoft Pseudopotentials to the Projector Augmented-Wave Method. *Phys. Rev. B: Condens. Matter Mater. Phys.* **1999**, *59*, 1758−1775.

(65) Dion, M.; Rydberg, H.; Schröder, E.; Langreth, D. C.; Lundqvist, B. I. Van der Waals Density Functional for General Geometries. *Phys. Rev. Lett.* **2004**, *92*, 246401.

(66) Klimeš, J.; Bowler, D. R.; Michaelides, A. Van der Waals Density Functionals Applied to Solids. *Phys. Rev. B: Condens. Matter Mater. Phys.* **2011**, *83*, 195131.

(67) Henkelman, G.; Uberuaga, B. P.; Jónsson, H. A Climbing Image Nudged Elastic Band Method for Finding Saddle Points and Minimum Energy Paths. *J. Chem. Phys.* **2000**, *113*, 9901−9904.

(68) Henkelman, G.; Jónsson, H. Improved Tangent Estimate in the Nudged Elastic Band Method for Finding Minimum Energy Paths and Saddle Points. *J. Chem. Phys.* **2000**, *113*, 9978−9985.

(69) Bader, R. *Atoms in Molecules: A Quantum Theory; International Series of Monographs on Chemistry*; Clarendon Press, 1994.

(70) Tang, W.; Sanville, E.; Henkelman, G. A Grid-based Bader Analysis Algorithm without Lattice Bias. *J. Phys.: Condens. Matter* **2009**, *21*, 084204.